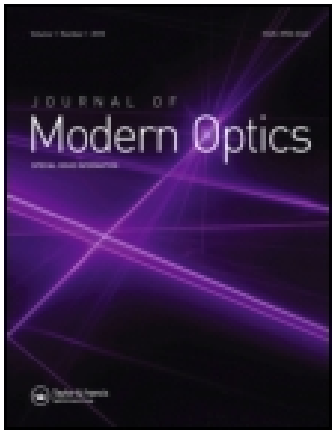

Journal of Modern Optics
Publication details, including instructions for authors and subscription information:
http://www.tandfonline.com/loi/tmop20

Novel methods to improve the measurement accuracy and the dynamic range of Shack-Hartmann wavefront sensor

Lei Yu[abc], Mingliang Xia[c], Hongsheng Xie[abc], Li Xuan[a] & Ji Ma[d]

[a] State Key Lab of Applied Optics, Changchun Institute of Optics, Fine Mechanics and Physics, Chinese Academy of Sciences, Changchun, China

[b] Graduate University of the Chinese Academy of Sciences, Beijing, China

[c] Medical Imaging Department, Suzhou Institute of Biomedical Engineering and Technology, Chinese Academy of Sciences, Jiangsu, China

[d] Liquid Crystal Institute, Kent State University, Kent, OH, USA

Published online: 28 Apr 2014.

To cite this article: Lei Yu, Mingliang Xia, Hongsheng Xie, Li Xuan & Ji Ma (2014) Novel methods to improve the measurement accuracy and the dynamic range of Shack-Hartmann wavefront sensor, Journal of Modern Optics, 61:9, 703-715, DOI: 10.1080/09500340.2014.909054

To link to this article: http://dx.doi.org/10.1080/09500340.2014.909054

Journal of Modern Optics, 2014
Vol. 61, No. 9, 703–715, http://dx.doi.org/10.1080/09500340.2014.909054

Novel methods to improve the measurement accuracy and the dynamic range of Shack–Hartmann wavefront sensor

Lei Yu[a,b,c]*, Mingliang Xia[c], Hongsheng Xie[a,b,c], Li Xuan[a] and Ji Ma[d]

[a]*State Key Lab of Applied Optics, Changchun Institute of Optics, Fine Mechanics and Physics, Chinese Academy of Sciences, Changchun, China;* [b]*Graduate University of the Chinese Academy of Sciences, Beijing, China;* [c]*Medical Imaging Department, Suzhou Institute of Biomedical Engineering and Technology, Chinese Academy of Sciences, Jiangsu, China;* [d]*Liquid Crystal Institute, Kent State University, Kent, OH, USA*

(*Received 6 December 2013; accepted 20 March 2014*)

As a wavefront sensor, the Shack–Hartmann wavefront sensor plays an important role in the wavefront measurement of human eyes. However, the low measurement accuracy and the small dynamic range of Shack–Hartmann wavefront sensor limit its application. In this paper, we present a matched-filter algorithm to improve the measurement accuracy by more than an order of magnitude. Moreover, we also introduce a new algorithm to extend the dynamic range of Shack–Hartmann wavefront sensor. With this method, the recorded spots of Shack–Hartmann wavefront sensor are not constrained to stay in the corresponding pixel area of the microlens. The result shows that the dynamic range can be extended from 57.1 to 160% for the first 24 items of Zernike wavefronts, respectively. The improvement by our methods makes the Shack–Hartmann more suitable for the measurement of highly aberrated eyes.

Keywords: Shack–Hartmann wavefront sensor; matched filter; ocular aberrations

1. Introduction

There is a long and storied history about the measurement of optical wavefronts. Classical interferometry requires a reference beam to measure a wavefront, while phase-retrieval methods learn as much as possible from one or more measurements of optical irradiance to reconstruct a wavefront [1,2]. Recently, various wavefront sensing techniques have been imposed on systems for ocular wavefront measurement [3–6]. Wavefront sensor plays an important role in understanding the optical quality of human eye and developing advanced visual correction techniques, such as adaptive optics, customized laser refractive surgery and customized contact lenses [7]. The laser ray-tracing technique, the spatially resolved refractometer and the Shack–Hartmann wavefront sensor are the most commonly used wavefront sensors [8–10]. The Shack–Hartmann wavefront sensor has proved to be reliable for ocular aberrations measurement [11]. Hence, the Shack–Hartmann wavefront sensor has a large number of ophthalmic applications, some of which have a great influence on the diagnosis of diseases [12–14].

The most important characteristics of Shack–Hartmann wavefront sensors are its measurement accuracy and dynamic range [15]. However, the classical centroiding algorithm has a poor precision and the dynamic range has also been questioned by other authors [16,17]. Generally, the noise without any significant information will corrupt the data recorded by the Shack–Hartmann wavefront sensor. Especially in the applications of ocular aberrations measurement, the multi-layer reflection of the eye leads to a complicated uneven background in the CCD data and makes it difficult to estimate the centroid positions. To overcome this obstacle, various methods have been introduced. These methods mainly consist of thresholding the data and applying a "software window" or Gaussian weighting function [18–20]. However, the threshold and the window size of these methods, which are adopted experientially, will also eliminate some significant information. This will bias the estimated centroid positions to some extent. In this paper, a matched filter algorithm is introduced to estimate the centroid positions without thresholding the CCD data. Since matched filter algorithm is more linear and less sensitive to noise than classical centroiding algorithm, the measurement accuracy of Shack–Hartmann wavefront sensor will be significantly improved by the matched filter algorithm [21–23].

On the other hand, the dynamic range of Shack–Hartmann wavefront sensor is limited by the parameter of microlens array. The classic methods require that the spots focused by the microlens must locate in the corresponding area of the CCD pixels. To extend the dynamic range, various algorithms are introduced, such as modified unwrapping algorithm and maximum likelihood methods [24–26]. In this paper, we also propose a new algorithm to extend the dynamic range of Shack–Hartmann wavefront sensor. This algorithm can

*Corresponding author. Email: yerlee@live.cn

effectively detect the spots which locate out of the corresponding area of the CCD pixels. Even if there are two spots locating in the same corresponding area of the CCD pixels, this algorithm still works well.

This paper is organized as follows: In Section 2, we discuss the techniques and methods of Shack–Hartmann wavefront sensor and its limits. Then we introduce the new algorithm to improve the measurement accuracy and the algorithm to extend the dynamic range of Shack–Hartmann wavefront sensor in Sections 3 and 4. In Section 5, we compare the result of new algorithms with that of classical methods. At last, we conclude this paper in Section 6.

2. Shack–Hartmann wavefront sensor and its limits

The Hartman wavefront sensor was first introduced in 1900. It consists of an opaque screen containing an array of holes and a detector placed behind the screen. The beam is sampled by the array screen and the transmitted beamlets are collected by the detector. The local aberrations of the beam cause a shift of the beamlets at the detector plane. By measuring the shifts in the x and y directions, the slope of the local wavefront can be determined. However, the measure accuracy of Hartmann wavefront sensor is very low and the loss of the light energy is very high. Hence, this kind of Hartmann is not suitable for measuring ocular aberrations. To solve this problem, R. Shack proposed a modified Hartmann wavefront sensor called Shack–Hartman wavefront sensor in 1971 [27]. In order to achieve smaller spot on the detector plane and increase the accuracy of wavefront measurement, the hole array screen is replaced by an array of microlens. All the microlenses of the array have the same diameter and the same focal length. As shown in Figure 1, the light reflected from the eye is distorted by the ocular aberrations. Then, the reflected light is sampled by the microlens array and forms a spot array in the focal plane of the microlens. The spot array is recorded by the CCD, which is placed at the focal plane of the microlens array, for wavefront reconstruction.

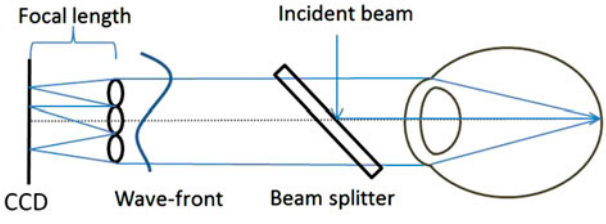

Figure 1. Schematic diagram of the principle of Shack–Hartmann wavefront sensor. (The colour version of this figure is included in the online version of the journal.)

As for the aberration-free case, the spots located at the focus of each microlens are shown in Figure 2(*a*).

However, the ocular aberrations in the emergent beam cause a measurable shift of the spots at the CCD plane, as shown in Figure 2(*b*). Moreover, the multilayer reflection of the eye adds a complicated uneven background to the spot array. The electronic noise without any significant information also corrupts the data.

The measurable shift of the spot from its aberration-free location is proportional to the slope of the local wavefront. Generally, the wavefront is expressed as a combination of Zernike polynomials:

$$\varphi(x,y) = \sum_{k=1}^{N} a_k \cdot z_k(x,y) + \varphi_0 \tag{1}$$

where $\varphi(x, y)$ is the wavefront at coordinate (x, y), $z_k(x, y)$ is the kth item of the Zernike polynomials and a_k is the kth coefficient of the Zernike polynomials. Since φ_0 is the constant item of the wavefront, the wavefront can be determined by the coefficient a_k.

On the other hand, the slope of the local wavefront can be expressed as:

$$\begin{aligned} G_{i,x} &= \frac{2\pi}{\lambda \cdot f} \cdot (x_i - x_{i,c}) \\ G_{i,y} &= \frac{2\pi}{\lambda \cdot f} \cdot (y_i - y_{i,c}) \end{aligned} \tag{2}$$

where $G_{i,x}$, $G_{i,y}$ are the x and y components of the slope of the local wavefront in the ith microlens, respectively. $(x_{i,c}, y_{i,c})$ is the centroid position of the aberration-free wavefront in the ith microlens while (x_i, y_i) is the centroid position of the local wavefront with ocular aberrations in the ith microlens. λ,f are the wavelength of the beam and the focal length of the microlens, respectively.

$G_{i,x}$, $G_{i,y}$ can also be expressed by:

$$\begin{aligned} G_{i,x} &= \sum_{k=1}^{N} a_k \cdot \frac{\partial z_k(x_i, y_i)}{\partial x} \\ G_{i,y} &= \sum_{k=1}^{N} a_k \cdot \frac{\partial z_k(x_i, y_i)}{\partial y} \end{aligned} \tag{3}$$

where $\frac{\partial z_k(x_i,y_i)}{\partial x}, \frac{\partial z_k(x_i,y_i)}{\partial y}$ are the x and y components of the derivative of Zernike polynomials. Hence, the ocular aberrations can be determined by calculating the centroid position of each spot in the spot array.

Generally, the centroid positions are calculated with a centroiding algorithm:

$$\begin{aligned} X_c &= \frac{\sum_{i=1}^{M}\sum_{j=1}^{N} x_i I(x_i, y_j)}{\sum_{i=1}^{M}\sum_{j=1}^{N} I(x_i, y_j)}, \\ Y_c &= \frac{\sum_{i=1}^{M}\sum_{j=1}^{N} y_j I(x_i, y_j)}{\sum_{i=1}^{M}\sum_{j=1}^{N} I(x_i, y_j)} \end{aligned} \tag{4}$$

where (X_c, Y_c) is the centroid position of the spot. $I(x_i, y_i)$ is the intensity of the beam at coordinate (x_i, y_i). M, N is

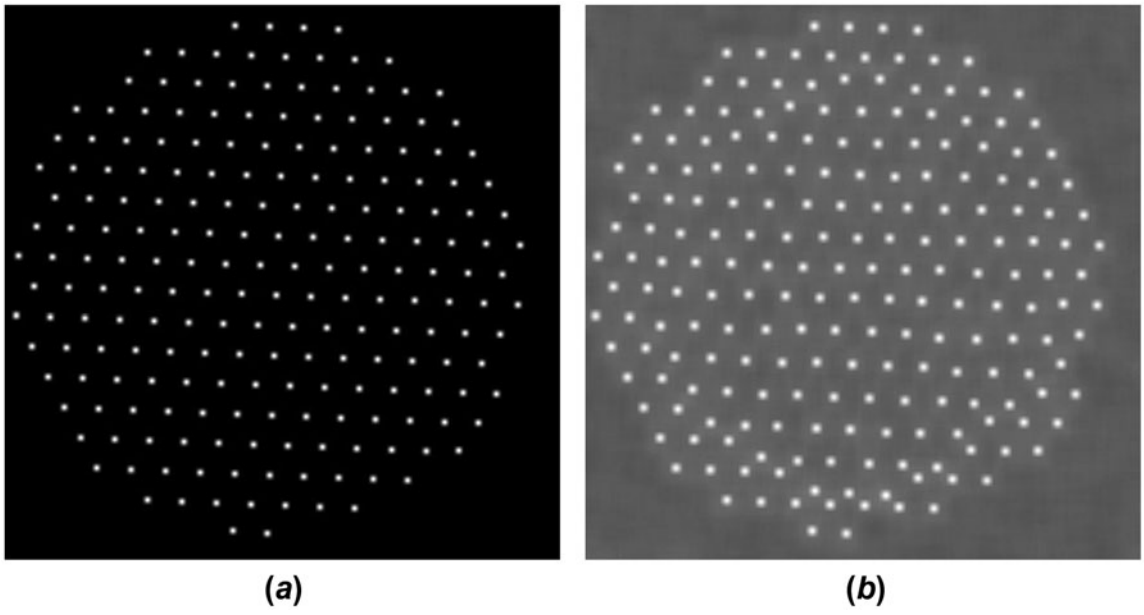

Figure 2. (*a*) Spot array of aberration-free eye; (*b*) Spot array of real eye.

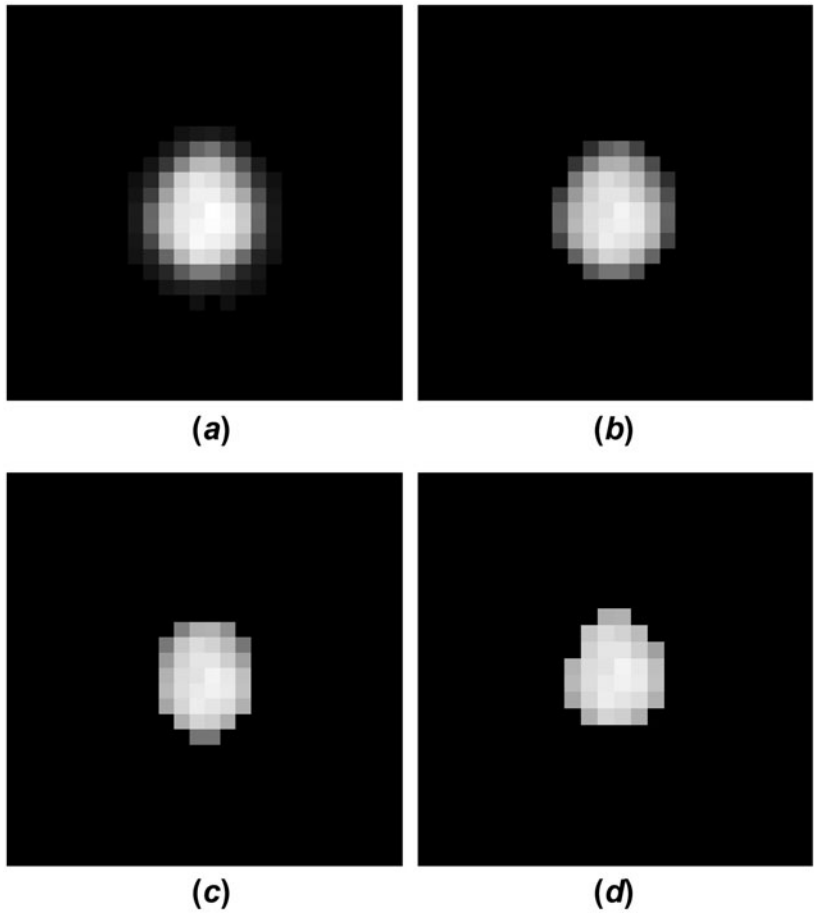

Figure 3. The same asymmetrical spot with different threshold. (*a*) $t = 0.1$; (*b*) $t = 0.3$; (*c*) $t = 0.5$; (*d*) $t = 0.7$.

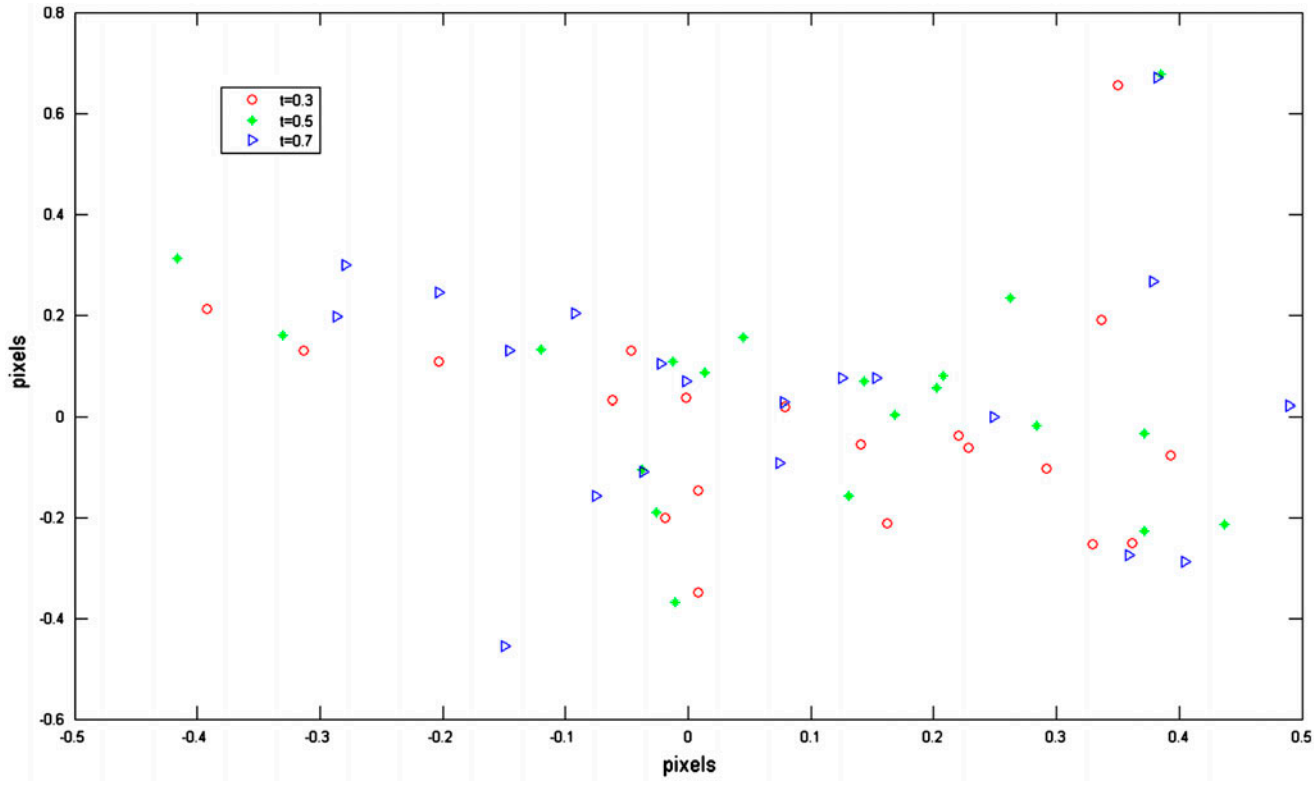

Figure 4. The effect of the noise level and the threshold. (The colour version of this figure is included in the online version of the journal.)

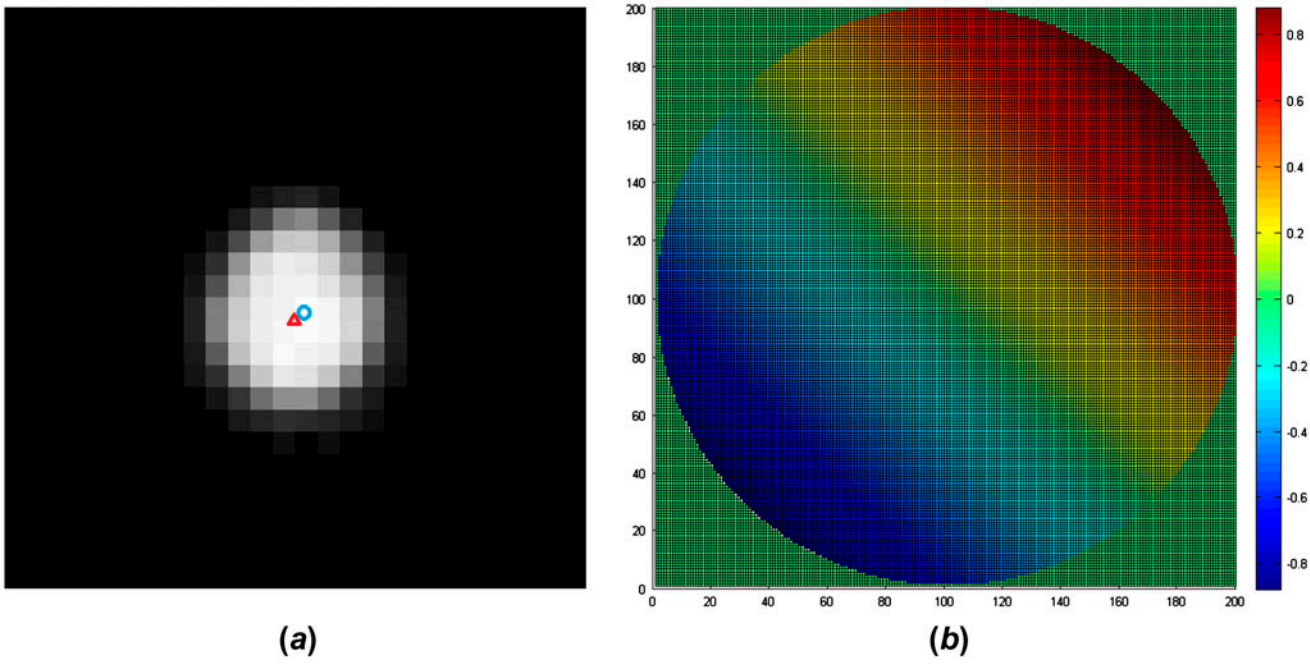

Figure 5. The effect of the Gaussian mask. (*a*) the centroid deviation; (*b*) the wavefront caused by the constant deviation. (The colour version of this figure is included in the online version of the journal.)

Table 1. Detailed parameters of the Shack–Hartmann wavefront sensor in the numerical simulation.

Size of microlens	0.3 mm
Focal of microlens	7.318 mm
Pixel size	2.5 μm
Number of microlenses	207
Wavelength of the beam	550 nm

the size of the "software window" containing the spot. However, this algorithm is sensitive to noise and the background light. With the existence of noise and background light, this centroiding algorithm leads to a biased estimation of the centroid position towards the centre of the "software window". To solve this problem, a threshold is always introduced to suppress the noise and the background light:

$$T = \left(\frac{2a}{3} - b\right) \cdot t + b \tag{5}$$

where T is the adaptive threshold. a, b are the maximum and the minimum of the local intensity, respectively. t is an experiential factor. It is introduced by Leroux C [28] to calculate the threshold for suppressing the background of spot array. The classical threshold algorithms always adopt an empirical threshold, which is relevant to the illumination and CCD performance. Expression (5) is a reasonable expression about the threshold algorithm. The a and b are the maximum and minimum of the local intensity, respectively. And t is an empirical factor between 0 and 1. When $t = 0$, $T = b$, there is no effective threshold of the spot array. On the other hand, when $t = 1$, $T = 2a/3$, it will suppress most of the background and the noises as well as some useful information. The Expression (5) assumes that $2a/3 > b$. This assumption will be met in most conditions. This threshold works well when the intensity of the incident beam is high enough. However, the intensity of the incident beam for ocular aberration measurement is very low because of the restriction of the secure exposure. Hence, the noise and the background light still corrupt the spot array data. Moreover, the spot of the ocular wavefront is asymmetrical as shown in Figure 3.

Because of the low intensity of the incident light, there is no significant boundary between the spot and the background light. Therefore, if the threshold is not high enough to effectively suppress the noise and the background light, the noise and background light will lead to a deviation from the real centroid position and increase the error of wavefront measurement. On the contrary, if the threshold is high enough to suppress the noise and the background light completely, it will increase the risk of losing the low-intensity pixels with significant information. This also increases the error of wavefront measurement. This effect of the threshold in centroid calculation is shown in Figure 4. The same asymmetrical spot is calculated by the centroiding algorithm with different noise levels and different thresholds. ○, ∗, Δ correspond to the experiential factor of the threshold $t = 0.3$, 0.5, 0.7, respectively. With the same experiential factor t, different noise levels lead to different deviations. With the same noise level, different values of the experiential factor t also lead to different deviations. Hence, the centroiding algorithm is sensitive to noise and background light. The measurement accuracy of centroiding algorithm is not satisfactory.

3. Matched filter algorithm

The matched filter algorithm evaluates the correlation between the spot array and the matched filter mask. The coordinate, which maximizes the local correlation of the spot array with the matched filter mask, denotes the centroid position of each spot. Generally, the matched filter mask, which has the same frequency information of the target in Fourier domain, will easily detect the target. However, the frequency information of the target is not available in practice. Since Gaussian can maintain the low frequency information, which denotes the significant information, and suppress the high frequency information, which denotes the noise, Gaussian distribution mask may be a reasonable choice.

If the spot is asymmetrical, the coordinate (the blue circle in the figure) that maximizes the local correlation of the spot array with the Gaussian mask deviates the real centroid (the red triangle in the figure) of the spot by a constant distance as shown in Figure 5(*a*).

Since the deviation is caused by the difference between the asymmetrical spot and the Gaussian mask rather than the noise and the background light, the deviation is constant for each spot. The constant deviation of each spot just leads to an extra tilt in the wavefront as shown in Figure 5(*b*). However, the first three items of the Zernike polynomials (piston, x-tilt and y-tilt) are generally not taken into account (The coefficients of these items are always set zero.) when measuring the ocular aberrations. Therefore, the constant deviation caused by Gaussian mask does not affect the ocular wavefront.

The correlation of the spot array with the Gaussian mask can be expressed as:

$$CR(x,y) = FT^{-1}\{FT\{I(x,y)\} \times FT\{G(x,y)\}\} \tag{6}$$

where $CR(x, y)$ is the correlation at coordinate(x, y). $I(x, y)$ is the spot array data while $G(x, y)$ denotes the Gaussian mask. Then, the coordinate that maximizes the correlation of the spot array with the Gaussian mask can be determined:

$$(x_i, y_i) = \arg\max CR(x,y) \tag{7}$$

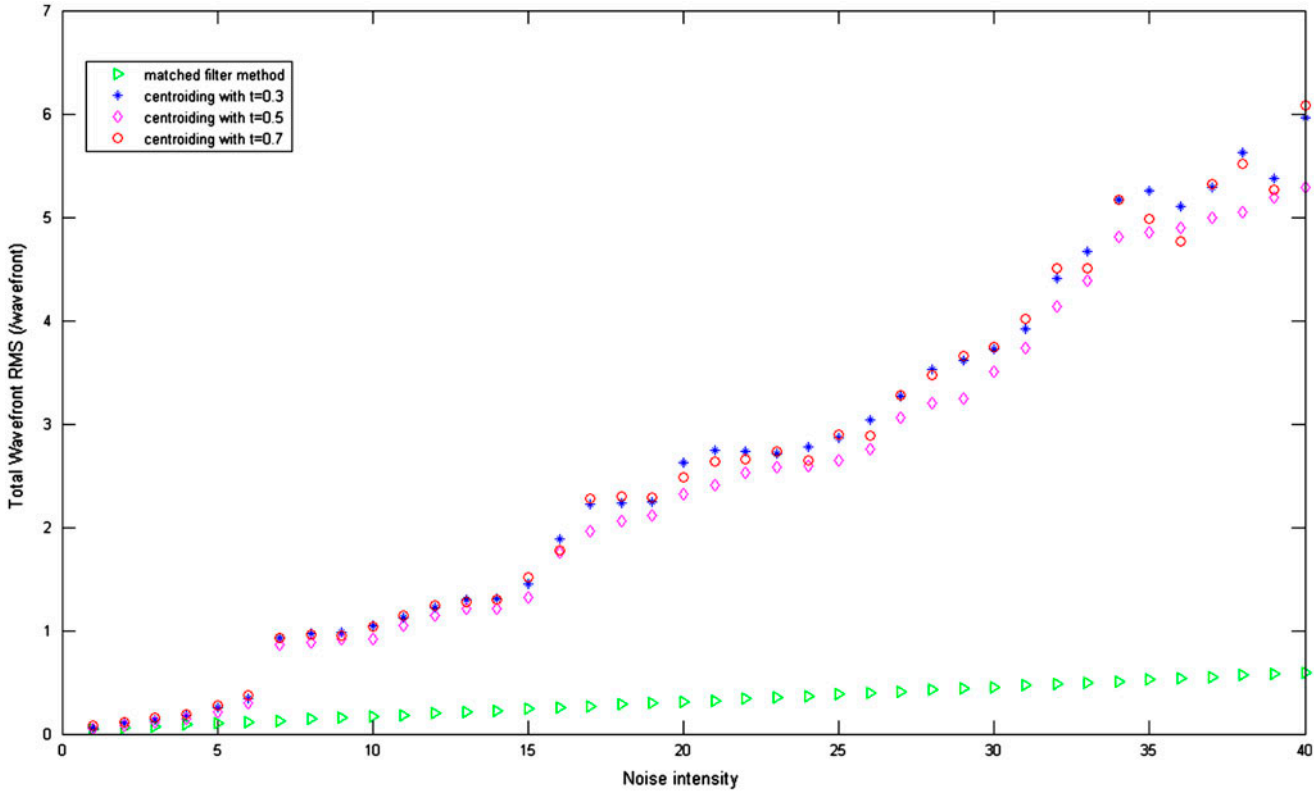

Figure 6. The accuracy of the matched filter algorithm and centroiding algorithm at different noise levels. (The colour version of this figure is included in the online version of the journal.)

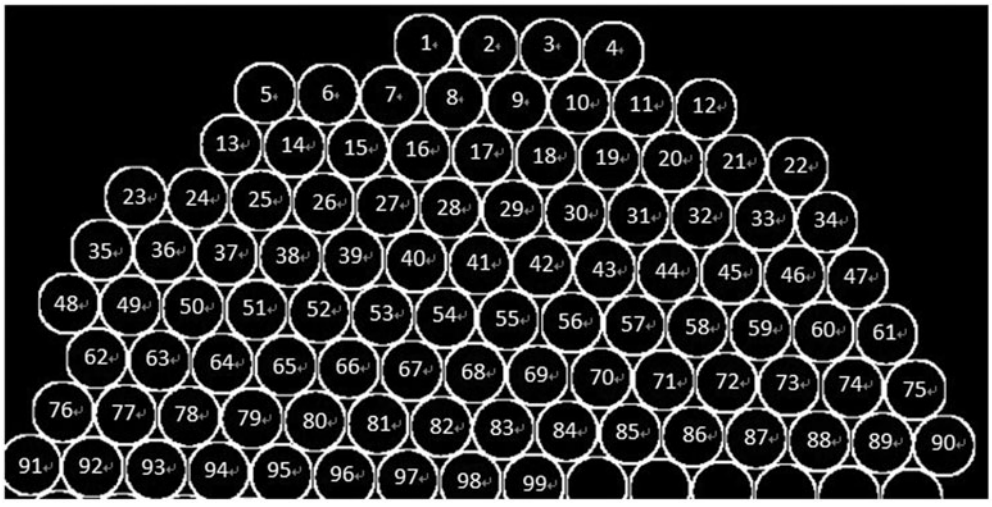

Figure 7. The number of the microlenses in the array.

As soon as one centroid position of spot is found, the local circular area of this spot in the correlation matrix $CR(x, y)$ is set zero. Then another centroid position of spot is calculated until all N centroids of the spot array are found. N is the number of microlenses.

This algorithm calculates the centroid positions of the spot array in the whole array data rather than in the corresponding pixel area of the microlens. Even if one spot locates out of the corresponding pixel area of the microlens, this algorithm can calculate the centroid position

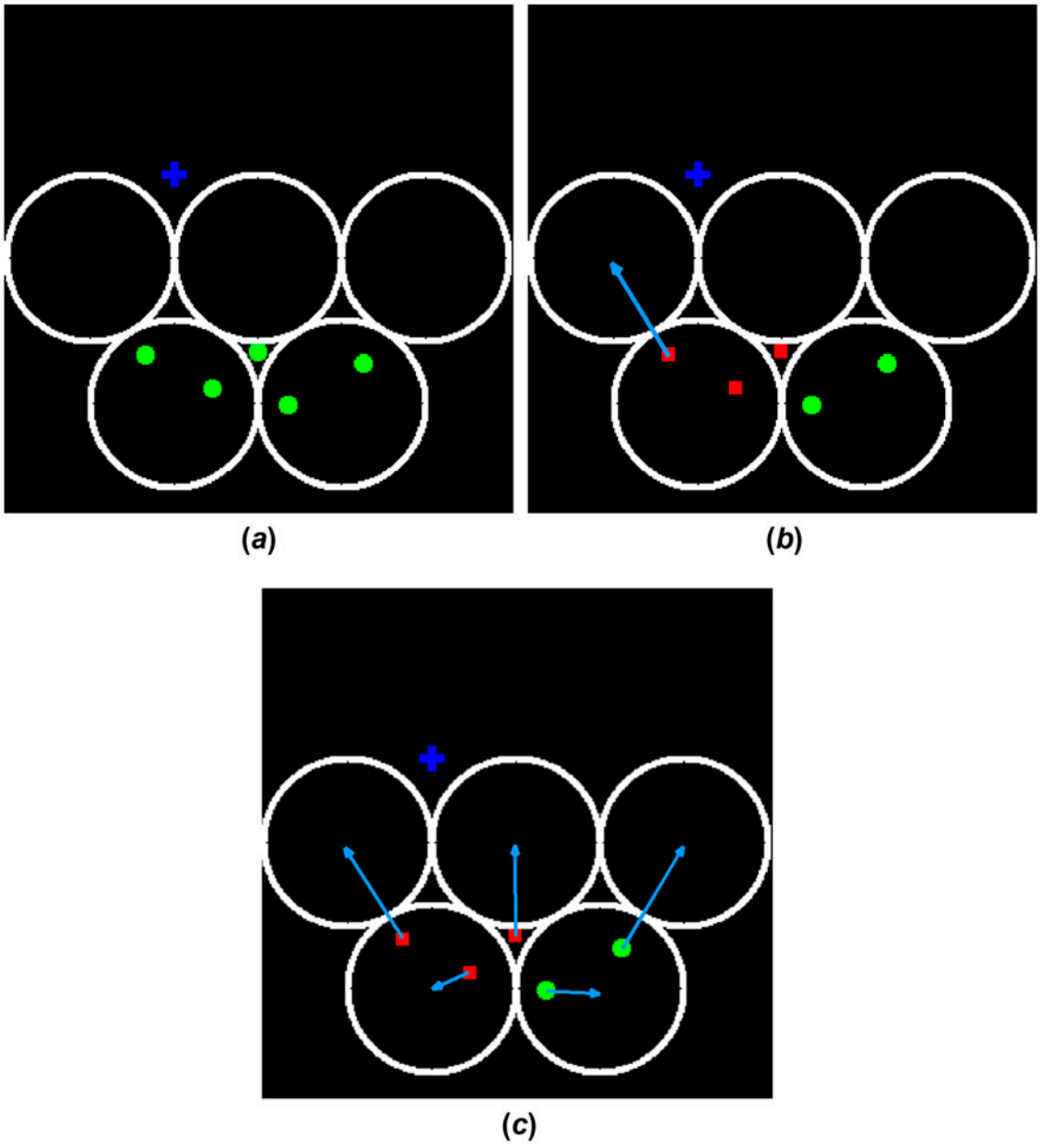

Figure 8. The process to relate the centroid array to the microlens array. (The colour version of this figure is included in the online version of the journal.)

of this spot correctly. Hence, this algorithm can also be used to extend the dynamic range of the Shack–Hartmann wavefront sensor. We will discuss a novel algorithm based on this algorithm to extend the dynamic range of the Shack–Hartmann wavefront sensor in detail in Section 4.

To illustrate the improvement of the measurement accuracy of Shack–Hartmann wavefront sensor, we present numerical simulations of the performances of this matched filter algorithm and the centroiding algorithm. The main parameters of this numerical simulation are summarized in Table 1.

The matched filter algorithm is sensitive to sampling frequency, so the pixel size should be small enough to maintain the accuracy and the linearity of this algorithm. If the pixel size is too big, the quantization error will corrupt the accuracy and the linearity of the matched filter algorithm. In this case, the centroid position of the spot should be determined by weighing the correlation response in a small window (3×3 pixels, for example) around the maximum of the correlation response. We compare the matched filter algorithm with the centroiding algorithm at different noise levels. The result is shown in

Figure 6. The intensity of the spot array data ranges from 1 to 255. In this case, the noise level is about 30 in practice. The total wavefront RMS is the sum of the RMS across the whole wavefront (200 × 200 pixels).

From Figure 6, we can find that there is no significant difference between the two algorithms when the noise level is low (less than 5). However, when the noise level gradually increases, the performance of the centroiding algorithm degrades sharply. This is because the threshold cannot distinguish the noise from the low-intensity signal in the spot array. On the other hand, the matched filter algorithm performs better than the centroiding algorithm by an order of magnitude, which is consistent with the conclusion of C. Leroux [28]. We can also find that the experiential factor impacts the performance of the centroiding algorithm. If the experiential factor is too small to suppress the noise ($t = 0.3$), the residual noise still corrupts the spot array data and leads to a bigger RMS than the case $t = 0.5$. On the contrary, if the experiential factor is too big ($t = 0.7$), the threshold will truncate the spot data and lead to loss of significant information. The total wavefront RMS of this case ($t = 0.7$) is also bigger than the case $t = 0.5$. Hence, the matched filter algorithm is more robust and accurate than the centroiding algorithm.

4. A novel algorithm to extend the dynamic range

As discussed in Section 3, the matched filter algorithm calculates the centroids of the spot array in the whole array data rather than in the corresponding pixel area of the microlens. By making use of this advantage, we introduce a novel algorithm to extend the dynamic range of Shack–Hartmann wavefront sensor in this section.

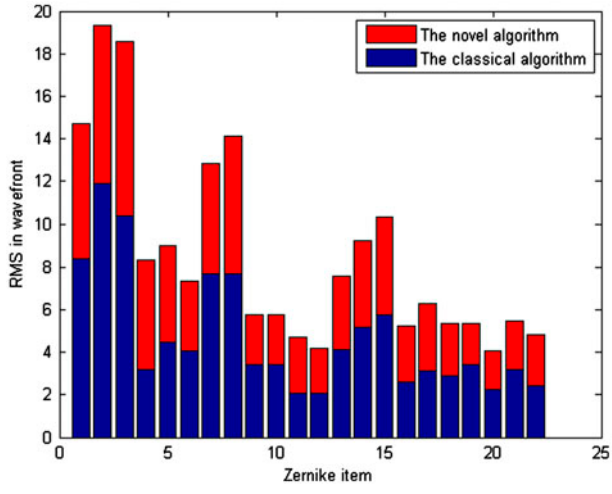

Figure 9. The dynamic range of the algorithms. (The colour version of this figure is included in the online version of the journal.)

The main purpose of this algorithm is to relate the centroid array with the microlens array. First of all, all the microlenses in the array should be numbered (by column or by row) as shown in Figure 7. The centroid positions of spots, which are calculated by the matched filter algorithm, should also be ordered by coordinate. Then the reference point of the ith microlens can be calculated as follows:

$$\begin{aligned} x_{i,r} &= x_{i,c} + 0.5r, \\ y_{i,r} &= y_{i,c} + 0.5r \end{aligned} \tag{8}$$

where $(x_{i,r}, y_{i,r})$ is the coordinate of the reference point. $(x_{i,c}, y_{i,c})$ is the coordinate of the centre of the ith microlens. r is the radius of the microlens.

The distance from the reference point to each of the centroid position is calculated as follows:

$$D_{i,j,r} = \sqrt{(x_{i,r} - x'_j)^2 + (y_{i,r} - y'_j)^2} \tag{9}$$

where $D_{i,j,r}$ is the distance from the reference point of the ith microlens to the jth centroid position. (x'_j, y'_j) is the coordinate of the jth centroid position. Then, the first N centroids, which minimize the distance $D_{i,j,r}$, are the potential centroids of the ith microlens. If (x'_j, y'_j) is the last centroid position in the row, $N = 1$, otherwise, $N = 3$.

If there is a crossover between two adjacent centroids, the wavefront cannot be reconstructed by just one picture of spot array. Therefore, we assume that there is no crossover between these centroids. The centroid position of the spot, which is focused by the ith microlens, can be determined as follows:

$$(x_i, y_i) = \arg\min\{x'_j, x'_j \in (x'_j, y'_j)\} \tag{10}$$

where (x_i, y_i) is the coordinate of the spot centroid, which is focused by the ith microlens. By repeating these calculations for every microlens, the centroid array can be related to the microlens array.

As shown in Figure 8, the blue cross denotes the reference point of the first microlens. The green spot is the centroid calculated by the matched filter algorithm. The first three centroids, which minimize the formula (9), are shown in Figure 8(b) as red square. According to the Equation (10), the centroid in the top left corner has the minimum abscissa. Hence, this centroid is the centroid of the spot focused by the first microlens. By repeating these processes, all of the centroids can be related to the microlens array as shown in Figure 8(c). Therefore, the wavefront can be reconstructed correctly.

5. Result

The dynamic range of the sensor is expressed as the largest RMS (Root Mean Square) of the wavefront, which can be measured correctly by this sensor. Since

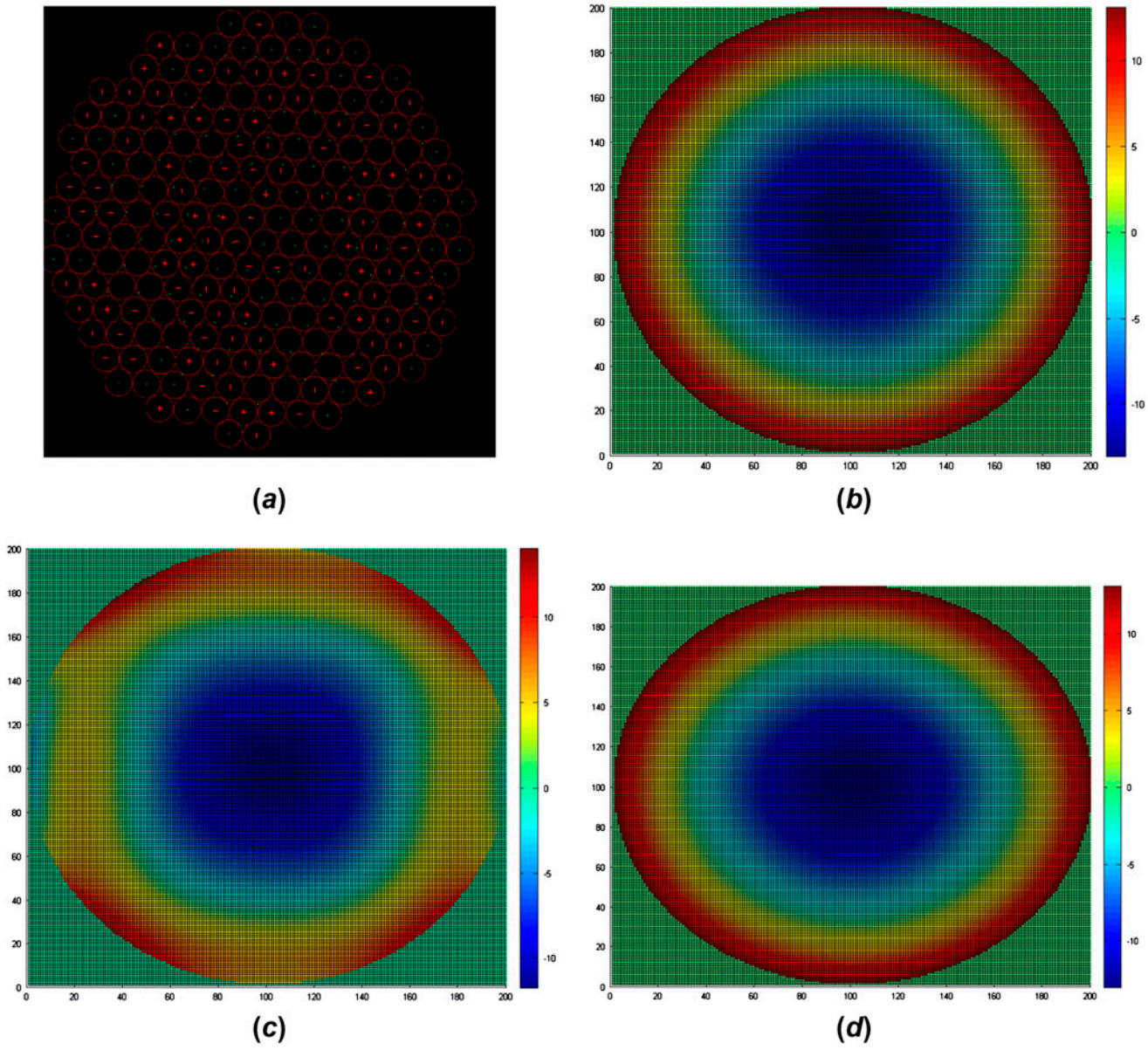

Figure 10. Z1,0 (*a*) Spot array (*b*) Reference wavefront (*c*) Wavefront reconstructed without our algorithm (*d*) Wavefront reconstructed with our algorithm. (The colour version of this figure is included in the online version of the journal.)

the RMS of the wavefront is proportional to the coefficient of the Zernike polynomials and the items of Zernike polynomials are orthogonal to each other [29], we can measure the dynamic range by increasing the coefficient of each item of Zernike polynomials while the coefficients of the other items remain zero. In the numerical calculation given, the real wavefront can be calculated from the coefficient of Zernike polynomials. And the spot array (without any noise) can be calculated from the coefficient of Zernike polynomials either. Then we reconstruct the wavefront with the spot array using both the classical algorithm and the proposed algorithm. We calculate the deviation between the reconstructed wavefront and the real wavefront. We increase the coefficient of Zernike polynomials until the deviation is above a given threshold (1% for example), then the dynamic range is exceeded. We regard the largest RMS of the real wavefront, the deviation between which and the reconstructed wavefront falls below the threshold, as the dynamic range of the sensor in the case of a single Zernike wavefront. The improvement of the dynamic range is calculated as:

$$\text{Improvement} = \frac{RMS_{\text{noval}} - RMS_{\text{classical}}}{RMS_{\text{classical}}} \qquad (11)$$

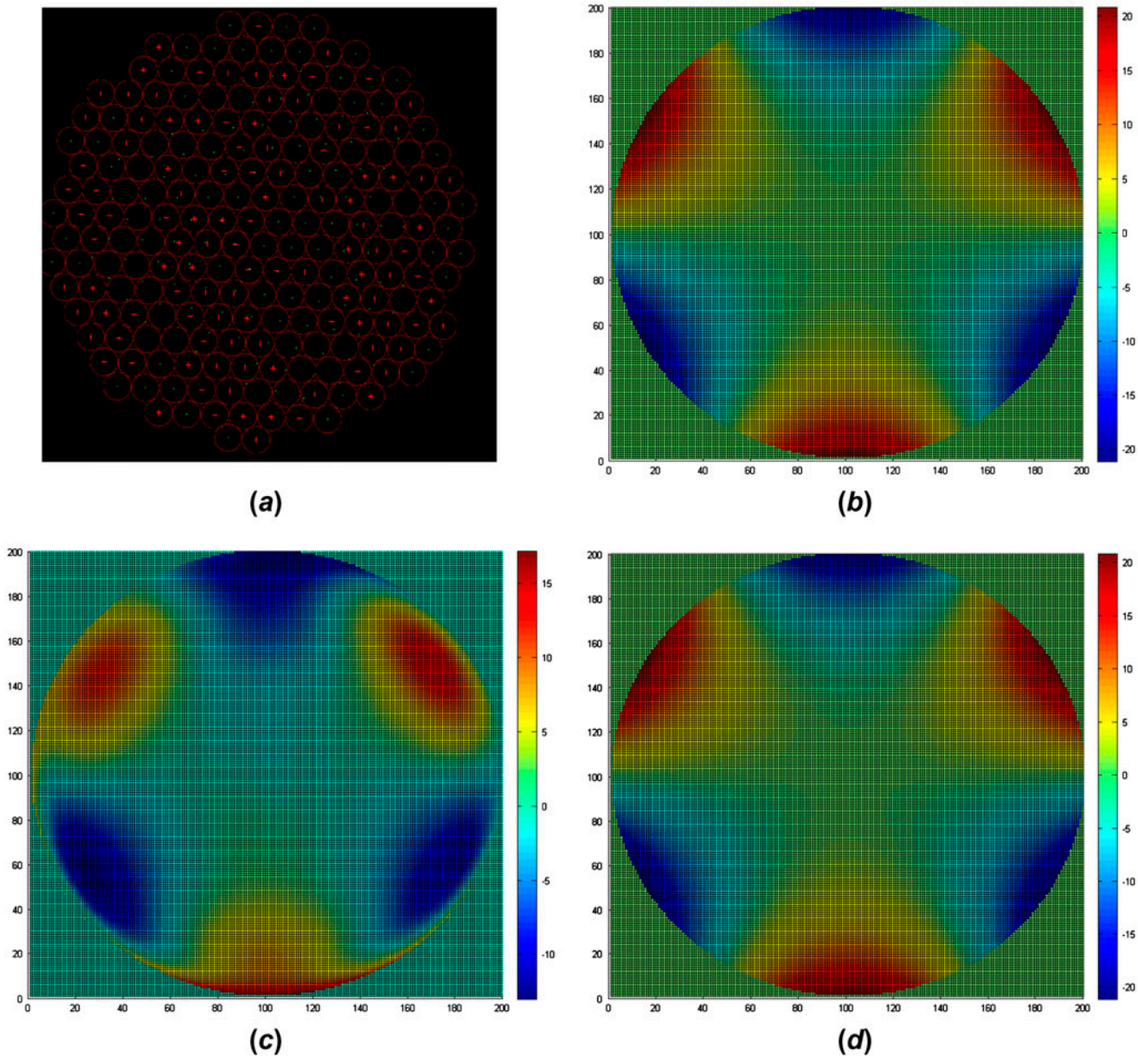

Figure 11. Z3,3 (*a*) Spot array (*b*) Reference wavefront (*c*) Wavefront reconstructed without our algorithm (*d*) Wavefront reconstructed with our algorithm. (The colour version of this figure is included in the online version of the journal.)

where RMS_{noval} and $RMS_{classical}$ are the largest RMS of the real wavefront, which can be correctly measured by the proposed algorithm and classical algorithm, respectively.

The dynamic ranges for the first 24 items of Zernike polynomials (without piston and tilt) are calculated with and without the novel algorithm. The result is shown in Figure 9. The improvement of the dynamic range for different items of Zernike polynomials ranges from 57.1 to 160% comparing to the classical algorithm.

The result of $Z_{1,0}$ and $Z_{3,3}$ are shown in Figures 10 and 11, respectively. From the spot array, we can find that some of the spots (the green dot in Figures 10(*a*) and 11(*a*)) are out of the corresponding pixel area of the microlens (the red circle in Figures 10(*a*) and 11(*a*)). In this case, the wavefront reconstructed by the classical algorithm is incorrect. Because the classical algorithm cannot relate the spot, which is out of the corresponding pixel area of the microlens, to the microlens, which focuses the spot. However, our algorithm can relate the

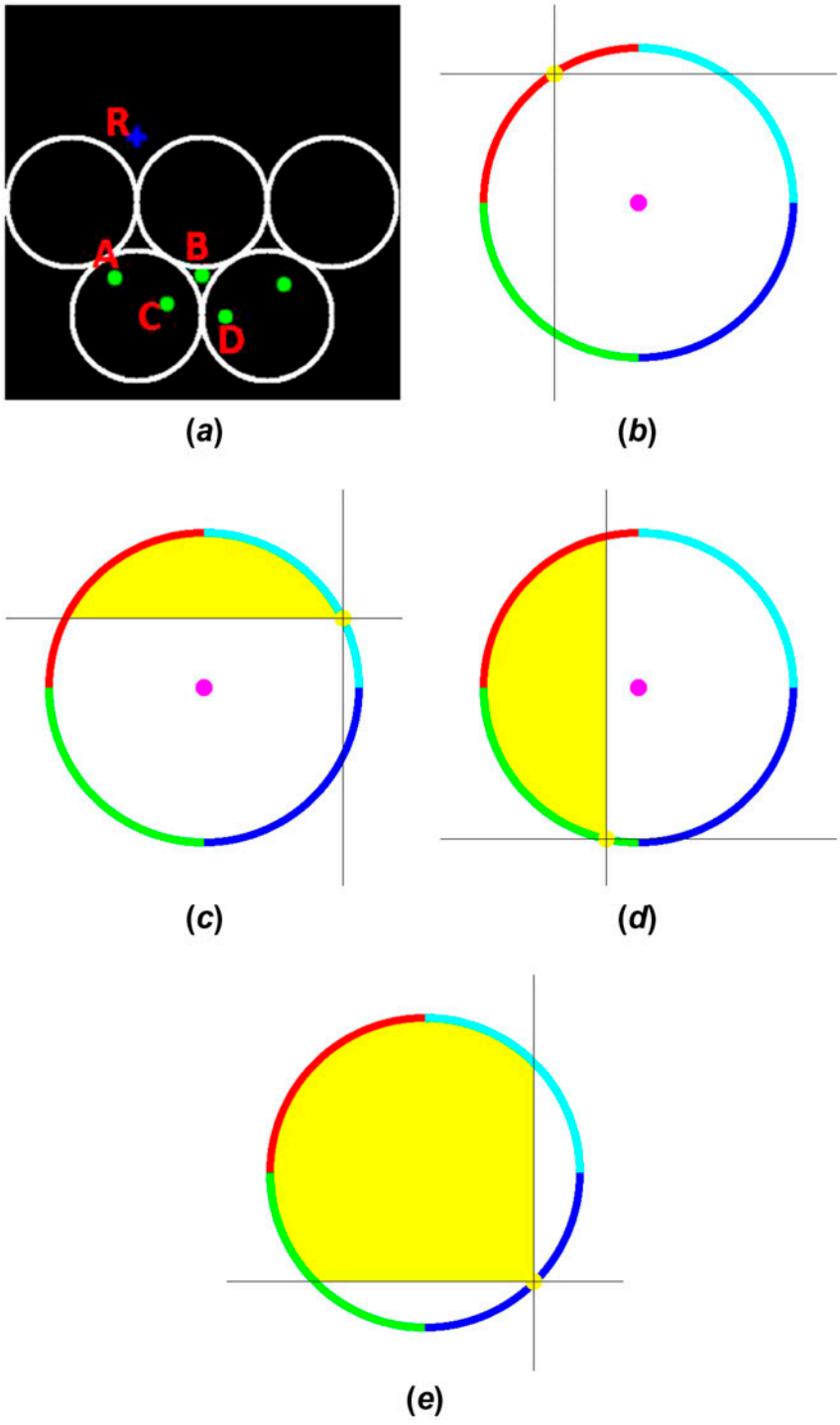

Figure 12. Limitations of the proposed algorithm: (*a*) the distribution of the microlens and spots; (*b*) there is no improvement when D locates at the second quadrant; (*c*) the improvement is moderate when D locates at the first quadrant; (*d*) the improvement is moderate when D locates at the third quadrant; (*e*) the improvement is large when D locates at the fourth quadrant. (The colour version of this figure is included in the online version of the journal.)

spot array to the microlens array in this case. Even if there are spots locating in the same microlens (as shown in Figure 11(*a*)), our algorithm can reconstruct the wavefront correctly. The error between the reconstructed wavefront and the reference wavefront is less than 10^{-12} wavelength.

Although the proposed algorithm can significantly improve the dynamic range of the Shack–Hartmann wavefront sensor, there are still some disadvantages: one of them is that, the spots should be bright enough to be visible and detectable. If there are some missing spots, the algorithm will fail. However, we can solve this problem by comparing the quantity of the microlens with that of spots. If the quantity of spots is not equal to that of microlens, there should be some missing spots and then another spot array will be acquired for calculation. It may cost a little extra time to acquire another spot array. But it is negligible when comparing to the calculation time.

The second disadvantage is that, even if there is no crossover in the spot array, this algorithm fails under some special conditions. As show in Figure 12(*a*), R is the reference point of the first microlens. A, B, C, D are the spots. Because there is no crossover in the spot array, the vertical coordinate of B is smaller than those of both C and D. The horizontal coordinate of C is smaller than those of both B and D. Now we think about the extreme case, B and C are too close to D, and they can be approximately regarded as one point. If the spot A is determined as potential centroid, then the algorithm works. Because there is no crossover between these spots, the horizontal coordinate of A is of course the minimum of those spots and will be determined by Expression (10). However, if the spot A is not regarded as potential centroid, the algorithm fails. In this case, the distance between A and R is longer than that between D and R. To illustrate this problem, we draw a circle with R as the centre. The radius is the distance between D and R. If A is outside the circle, the algorithm fails. Therefore, A must be inside the circle. On the other hand, both the horizontal coordinate and the vertical coordinate of A are smaller than those of D. Because there is no crossover between these spots. Therefore, A must locate at the second quadrant in the coordinate system with D as origin point. When D is located at a different quadrant of the coordinate system with R as origin point, the potential location of A is different and is shown in Figure 12(*b*)–(*e*), respectively (yellow area inside the circle).

From the figure, we can find that: (1) When D locates at the second quadrant of the coordinate system with R as origin point (as the yellow point shown in Figure 12(*b*)), the area of the potential location of A is zero, that is the algorithm will definitely fail in this case. (2) When D locates at the first or the third quadrant of the coordinate system with R as origin point (as the yellow point shown in Figure 12(*c*) and (*d*)), the area of the potential location of A is moderate, that is the proposed algorithm can improve the dynamic range of the sensor to some extent. (3) When D locates at the fourth quadrant of the coordinate system with R as the origin point (as the yellow point shown in Figure 12(*e*)), the area of the potential location of A is large, that is the proposed algorithm can improve the dynamic range of the sensor significantly. Because the reference point R locates at the top left direction of the microlens, which generates the spot D, the normal case is case (3). This is consistent with the numerical result. The improvement of the dynamic range is up to 160%. The case (2) sometimes happens, this is why the improvements of different items of Zernike polynomials are different from each other. The case (1) rarely happens, in this case spot B, C and D all locate at the top left of the microlens, which generates the spot A. In the case of ocular aberration measurement, local wavefront tilt would not be so large. There must be a global tilt in the wavefront, because all of the spot B, C and D are shifted significantly to the same direction. The global tilt can be compensated by tilt mirror. An easier way is to neglect the global tilt item of the Zernike polynomials. As discussed above, even if when there is a large local wavefront tilt, the proposed algorithm fails, the improvement of the dynamic range is significant when the local wavefront tilt is moderate. The defocus and global tilt items of the Zernike polynomials are compensated by lens. Therefore, this algorithm works well in our system in the case of ocular aberration measurement.

6. Conclusion

The Shack–Hartmann wavefront sensor has a large number of applications. However, the measurement accuracy and the dynamic range of the Shack–Hartmann wavefront sensor have been questioned by many other authors. In this paper, we have introduced a novel algorithm to estimate the centroid positions. This algorithm is based on matched filter algorithm. As shown in the experimental results, the measurement accuracy of our algorithm is better than the classical centroiding algorithm by an order of magnitude. Our algorithm is less sensitive to noise and more robust than the classical algorithm. Basing on the novel centroiding algorithm, we have also introduced an algorithm to extend the dynamic range of the Shack–Hartmann wavefront sensor. The classical centroiding algorithm calculates the centroid positions of the spots only in the corresponding pixel area of each microlens. Hence, if there is any spot locating out of the corresponding pixel area of the microlens, the reconstructed wavefront will be incorrect. However, our algorithm calculates the centroids of the spot array in the whole array data and can effectively relate the spot array to the microlens array. As shown in the experimental results, the dynamic ranges of the Shack–Hartmann wavefront sensor for the first 24 items of Zernike polynomials are significantly improved by our algorithm. The improvement of the dynamic range

ranges from 57.1 to 160% for different items of Zernike polynomials. Even if there are two or more spots locating in the corresponding pixel area of the same microlens, our algorithm works correctly. The error between the reconstructed wavefront and the reference wavefront is less than 10^{-12} wavelength.

The algorithms proposed in this paper also have some shortcomings: First of all, our algorithms are more complicated than the classical algorithms. Hence, they will cost more time to reconstruct the wavefront. However, this problem can be solved by improving the property of the computer. Secondly, if there is a crossover between two spots in the spot array, our algorithm cannot detect the crossover and may reconstruct the wavefront incorrectly. This problem cannot be solved only by a picture of spot array. To overcome this obstacle, a series of spot arrays before and after the crossover should be acquired.

Although our algorithms have these drawbacks, the experimental results show that the measurement accuracy and the dynamic range of the Shack–Hartmann wavefront sensor are both improved significantly. Thus, our algorithms should be effective enough to measure the aberrations of highly aberrated eyes.

Funding

This work was supported by the National Natural Science Foundation of China [60736042], [1174279], [1174274].

References

[1] Ge, Z.; Saito, T.; Kurose, M.; Kanda, H.; Arakawa, K.; Takeda, M. *Opt. Express* **2008,** *16,* 133–143.
[2] Li, M.; Li, X. *Opt. Express* **2009,** *17,* 15257–15263.
[3] Iglesias, I.; López-Gil, N.; Artal, P. *J. Opt. Soc. Am. A.***1998,** *15,* 326–339.
[4] Walsh, G.; Charman, W.; Howland, H. *J. Opt. Soc. Am. A* **1984,** *1,* 987–992.
[5] Navarro, R.; Mereno, E.; Dorronsoro, C. *J. Opt. Soc. Am. A* **1998,** *15,* 2522–2529.
[6] He, J.; Marcos, S.; Webb, R.; Burns, S. *J. Opt. Soc. Am. A* **1998,** *15,* 2449–2456.
[7] Porter, J.; Queener, H.; Lin, J.; Thorn, K.; Awwal, A. *Adaptive Optics for Vision Science: Principles, Practices, Design, and Applications*; John Wiley: Hoboken, NJ, **2005**.
[8] Navarro, R.; Losada, M. *Optom. Vis. Sci.* **1997,** *74,* 540–547.
[9] Webb, R.; Penney, C.; Thompson, K. *Appl. Opt.* **1992,** *31,* 3678–3686.
[10] Liang, J.; Williams, D. *J. Opt. Soc. Am.* **1997,** *14,* 2873–2883.
[11] Liang, J.; Grimm, B.; Goelz, S.; Bille, J. *J. Opt. Soc. Am. A.* **1994,** *11,* 1949–1957.
[12] Rahman, S.; Booth, M. *Appl. Opt.* **2013,** *52,* 5523–5532.
[13] Choi, W.; Baumann, B.; Swanson, E.; Fujimoto, J. *Opt. Express* **2012,** *20,* 25357–25368.
[14] Merino, D.; Dainty, C. *Opt. Express* **2006,** *14,* 3345–3353.
[15] Ríos, S.; López, D. *Opt. Express* **2009,** *17,* 9669–9679.
[16] Bara, S.; Prado, P.; Arines, J.; Ares, J. *Opt. Lett.* **2006,** *31,* 2646–2648.
[17] Llorente, L.; Marcos, S.; Dorronsoro, C.; Burns, S. *J. Opt. Soc. Am. A.* **2007,** *24,* 2783–2796.
[18] Ares, J.; Arines, J. *Opt. Lett.* **2001,** *26,* 1831–1833.
[19] Ares, J.; Arines, J. *Appl. Opt.* **2004,** *43,* 5796–5805.
[20] Baker, K.; Moallem, M. *Opt. Express* **2007,** *15,* 5147–5159.
[21] Gilles, L.; Ellerbroek, B. *Opt. Lett.* **2008,** *33,* 1159–1161.
[22] Ruggiu, J.; Solomon, C.; Loos, G. *Opt. Lett.* **1998,** *23,* 235–237.
[23] Gilles, L.; Ellerbroek, B. *Appl. Opt.* **2006,** *45,* 6568–6576.
[24] Leroux, C.; Dainty, C. *Opt. Express* **2009,** *17,* 19055–19061.
[25] Pfund, J.; Lindlein, N.; Schwider, J. *Opt. Lett.* **1998,** *23,* 995–997.
[26] Barrett, H.; Dainty, C.; Lara, D. *J. Opt. Soc. Am. A.* **2007,** *24,* 391–414.
[27] Platt, B.; Shack, R. *History and principles of Shack-Hartmann wavefront sensing*. 2nd Int. Congress of Wavefront Sensing and Aberration-free Refractive Correction (Monterey, California) **2001,** *17*, (America Slack Inc.) S573–77.
[28] Leroux, C.; Dainty, C. *Opt. Express* **2010,** *18,* 1197–1206.
[29] Wyant, James.C. *Zernike polynomials*, **2003**. ZernikePolynomialsForTheWeb.nb